

Buckling of coped steel beams and steel beams with partial endplates

Johan Maljaars^{1,2}, Jan W.B. Stark³ and Henri M.G.M. Steenbergen¹

¹ TNO Environment and Geosciences, Delft, The Netherlands

² Faculty of Architecture, Building and Planning, Technical University of Eindhoven, Eindhoven, The Netherlands

³ Faculty of Civil Engineering and Geosciences, Delft University of Technology, Delft, The Netherlands

Copes and partial endplates influence the resistance to lateral buckling of a steel beam. In order to quantify this influence, numerical research has been carried out with validated models. Full-scale laboratory tests carried out for the validation of the numerical models are described in the Annex to this paper.

The research resulted in proposed reduction factors for the critical elastic buckling load of beams with various end connections. With the reduced elastic buckling load and the existing buckling curves the resistance of steel beams with copes and partial end plates can be determined.

Keywords: *Lateral-torsional buckling, cope, endplate, steel, beams, buckling*

1 Introduction to lateral-torsional buckling

Beams loaded about the strong axis may buckle, which is called lateral-torsional buckling or flexural torsional buckling. The well-known, analytically derived equation for the critical elastic buckling load (M_{cr}) of a simply supported beam, loaded by a moment which is constant along the span (equation 1) was published by Timoshenko and Gere in 1960 (16). (Symbols used are listed at the end of this paper).

$$M_{cr} = \frac{\pi}{L} \sqrt{EI_z \left(GI_t + \frac{\pi^2}{L^2} \right) EI_{wa}} \quad (1)$$

Equation 1 shows that the moment of inertia about the weak axis, the torsional constant and the warping constant are parameters that determine the resistance to buckling, together with the span. I-sections are often used as beams because of the favourable ratio between resistance and weight. A disadvantage of I-sections, however, is that they have a relatively low critical elastic buckling load because of the relatively low torsional constant, the low warping constant and the small ratio between I_y and I_z .

In figure 1, the relation between the critical elastic buckling load and the resistance of a beam is illustrated. The horizontal axis in this figure represents the lateral deflection of the cross-section at mid-span of a simply supported beam loaded by a concentrated load applied at mid-span. The beam load is shown on the vertical axis and the graphs show results of finite element calculations. The solid black line represents the (post) buckling behaviour of an initially perfect I section loaded by a concentrated load at mid span. No lateral deflection occurs for loads smaller than the critical elastic buckling load M_{cr} . For a load equal to the critical elastic buckling load, lateral deflections occur and the magnitude of the lateral deflection is undetermined (instability). For a beam with (small) initial geometric imperfections (dashed line), lateral deflection occurs from the beginning of loading. The lateral deflection becomes significant for a load approaching the critical elastic buckling load, and is greater than in case of the perfect beam for every load. When the plastic capacities are determined of laterally restrained beams with various values for the initial geometric imperfection, it turns out that the maximum load decreases as the initial geometric imperfection increases (dotted line, each dot represents a beam with specific initial imperfection). As a result, the load displacement diagram of a laterally unsupported beam with a certain yield stress, initial geometric imperfections and residual stresses (solid grey line) shows a maximum load, which is the beam resistance. Residual stresses reduce the resistance in case of lateral-torsional buckling. For the considered beam, the resistance is lower than both the plastic capacity and the critical elastic buckling load.

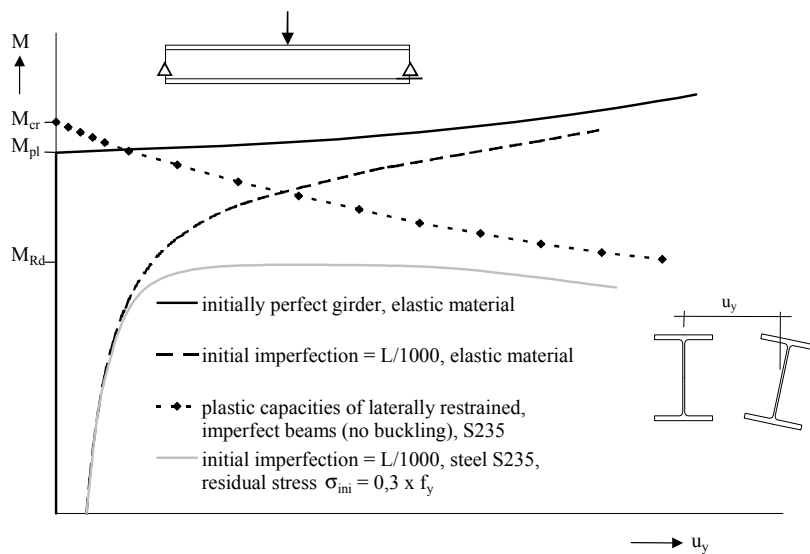


Figure 1: Relation between resistance, critical elastic buckling load and plastic capacity

In this example, the critical elastic buckling load was slightly lower than the plastic capacity. For beams with a much higher critical elastic buckling load, buckling does not significantly influence the beam resistance. The resistance of such beams is dominated by the plastic capacity, whereas for beams with a much lower critical elastic buckling load, the beam resistance is dominated by buckling. In codes such as prEN 1993-1-1 (19) the influence of the critical elastic buckling load on the beam resistance is expressed as a function of the relative slenderness λ_{LT} , see equation (2).

$$\lambda_{LT} = \sqrt{\frac{M_{pl}}{M_{cr}}} \quad (2)$$

Figure 2 shows the ratio between the beam resistance and the plastic capacity (χ_{LT}) as a function of the relative slenderness (λ_{LT}). For a beam with large slenderness, the critical elastic buckling load (solid black line) dominates the resistance, while the plastic capacity (grey line) dominates the resistance for stocky beams. The influence of initial imperfections is taken into account by the use of a buckling curve. In prEN 1993-1-1 (19), buckling curve 'a' (dashed line) is used for the design resistance of rolled sections. This buckling curve is based on the results of many tests. As shown, the influence of initial geometric imperfections and residual stresses on the resistance is largest when the critical elastic buckling load is equal to the plastic capacity (at a relative slenderness equal to 1).

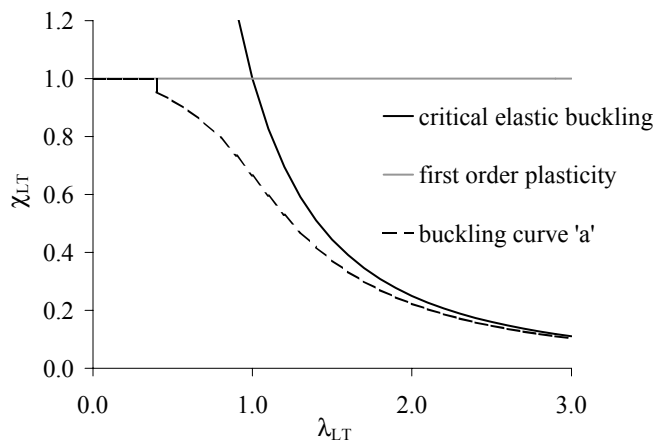


Figure 2: Buckling curve 'a' according to prEN 1993-1-1

2 Influence of support conditions on lateral-torsional buckling

Equation (1) is derived for a beam with simple supports, i.e. the rotation about the longitudinal axis and lateral and the vertical deflections are completely restrained, while the rotation about the strong and weak axes is free. In addition, the beam ends are assumed free to warp, but no other distortion

of the beam ends is present. These theoretical support conditions are not fulfilled in most real connections with e.g. endplates, fin plates or angles. Trahair and others [Trahair, 1993 (17), Pi and Trahair, 2000 (15) and Vacharajittiphan and Trahair, 1974 (18)] studied the effect of partial restraints at the supports on the critical elastic buckling load. They determined the increase of M_{cr} caused by partial restraints to rotations about the weak axis and the strong axis and by restrained warping (e.g. in case of thick, full endplates). They also determined the reduction of M_{cr} caused by partial restraint to rotation about the longitudinal axis. Based on these and on other studies, modification factors for the critical elastic buckling load are given in prEN 1993-1-1 to take into account the influence of partial restraints at the supports.

In practice, secondary beams are sometimes coped at the connection with main beams, see figure 3. The reason for coping beams is to allow the upper flanges of both beams to be levelled, so that it is possible to attach roof or floor plates without having to make additional modifications. The connection between main beam and secondary beam is made with endplates, fin plates or angles. Applying these connections may influence the lateral buckling resistance of the beam.

Local web buckling in the coped region or lateral-torsional buckling of the coped region may occur. This may reduce the critical elastic buckling load.

Web buckling may also occur in uncoped ('normal') beams when partial endplates are used, so that the upper flange and / or lower flange are not supported. Figure 4 illustrates that the buckling mode is a combination of local web buckling or buckling of the coped region and lateral-torsional buckling (only half of the beam is shown).

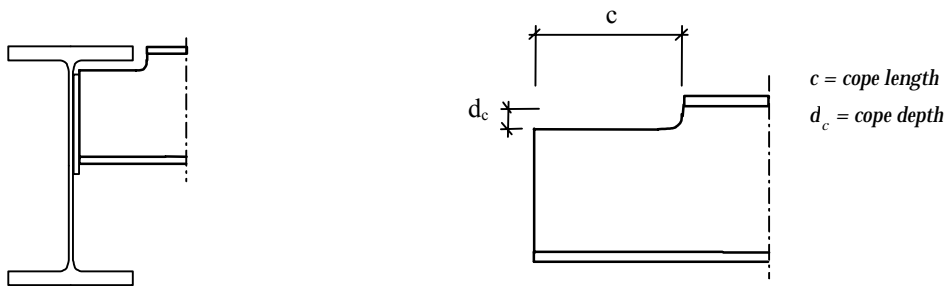


Figure 3: Coped connection between two beams

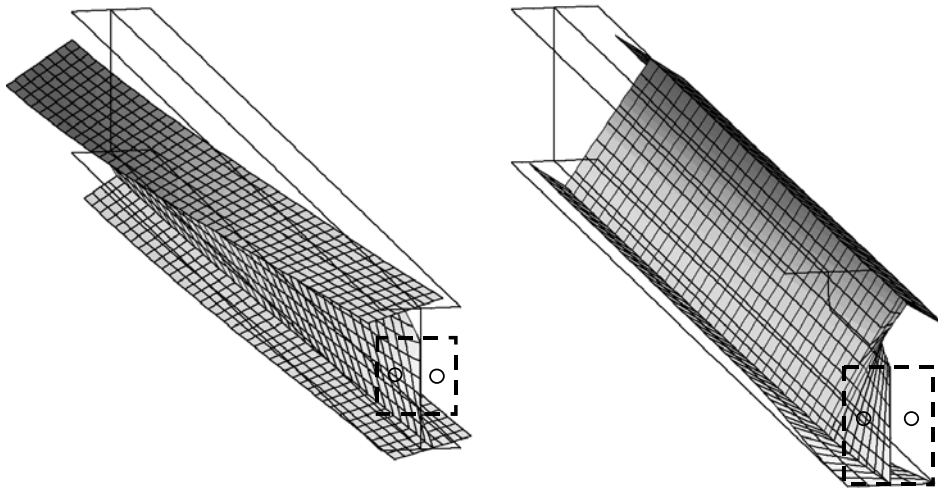


Figure 4: Buckling of a beam with short endplates (left) and a coped beam (right)

Figure 5 shows the results of finite element calculations of beams with the same span, load, initial imperfections and yield stress but with different support conditions. It is shown that both the resistance and the post critical deformation decrease as the beam end is less supported.

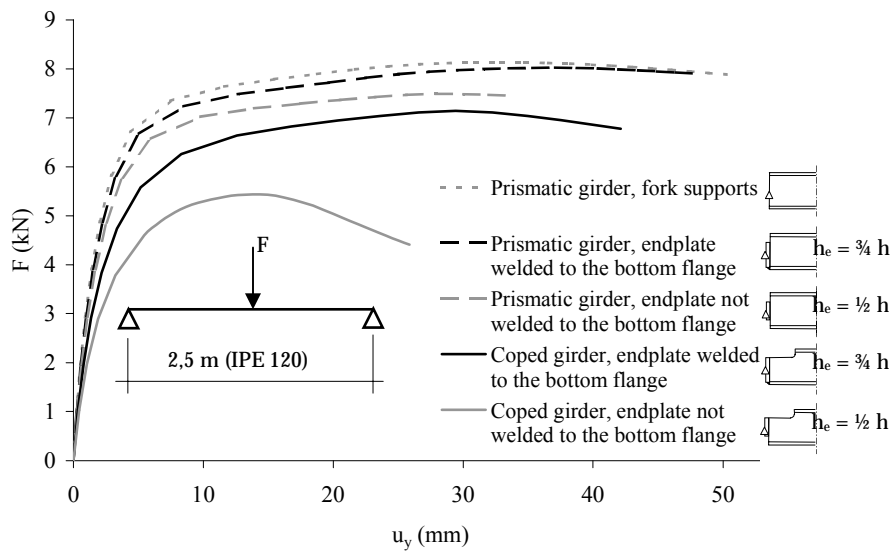


Figure 5: Difference in resistance and post critical behaviour due to end conditions

Numerical research into the influence of copes on the critical elastic buckling load has been carried out by Cheng, Yura and Johnson, 1988 (4), Lam, Yam, Iu and Cheng, 2000 (5) and Abspoel and

Stark, 1999 (1, 2). The research projects concentrated on I-section beams loaded by a concentrated load at mid-span. The results showed that for slender coped beams, buckling of the beam is dominated by lateral-torsional buckling, while buckling of a stocky coped beam is dominated by buckling of the coped region. For stocky beams with large cope length to web depth ratios, instability of the cope occurs by lateral-torsional buckling of the coped region, while in case of stocky beams with small cope length to web depth ratios, instability of the cope occurs by local web buckling in the coped region.

The research projects resulted in various equations for the critical elastic buckling load of coped beams.

Physical tests were carried out by Du Plessis, 1977 (14), Cheng and Yura, 1988 (3), Lindner, 1982 (10), Lindner, 1985 (12), Lindner and Gietzelt, 1985 (7), Lindner, 1987 (11), Lindner, 1988 (9) and Lindner, 1996 (8). The (coped) beams in these research projects were supported by main beams or frames. As a result, the beam ends of the tested beams were partially restrained to rotations about the weak and strong axes. The tests showed a reduction in resistance due to copes. Lindner, 1988 (9) presented graphs for the reduction in resistance due to partial endplates and copes, based on test results.

The tests could not directly be used to validate the numerical models because of the following reasons:

- The models developed so far were used to determine the critical elastic buckling load, while in tests the resistance is determined;
- The actual dimensions of the cross-section and the size of the geometric imperfections of the tested beams were not measured. These parameters influence the beam resistance;
- The numerical models were simply supported while partial restraints were applied in the laboratory tests;

Besides, the relatively large contribution of the roots at flange-web junctions to the rotation stiffness of the beam was not included in the numerical models developed so far.

The following general criteria apply for studying the reduction in beam resistance due to copes or partial endplates.

1. In the numerical models, the contribution to the rotation stiffness provided by the roots at flange-web junctions should be taken into account;
2. Numerical models should not only provide the critical elastic buckling load, but also the beam resistance including the influence of plasticity, residual stresses, large displacements and initial geometric imperfections;
3. Numerical models should be validated by tests;

4. The influence of real end connections by (partial) endplates, fin plates and angles on buckling of coped beams should be taken into account;
5. Partial restraints of the beam ends, provided by the main beam or frame to which the coped beam is connected should be taken into account;
6. Other load conditions than a concentrated load, applied at mid-span should be considered.

In the current research project, numerical models of simply supported (coped) beams with endplates loaded by a concentrated load or a uniformly distributed load were developed. The end connections according to figure 6 were modelled.

- Type 1 Standard conditions of restraint or fork supports. These conditions do not represent a real connection, but are used as the reference case. These end conditions are as applied for the derivation of equation 1;
- Type 2 Connections with endplates that support the bottom flange and at least a part of the web. The upper flange is not supported;
- Type 3 Connections with partial endplates that support only a part of the web and leave both flanges unsupported.
- Type 4 Connections with full endplates in combination with copes at the beam ends. The endplate is welded to the total web and the bottom flange and therefore supports the entire beam end.
- Type 5 Connections with partial endplates in combination with copes at the beam ends. The endplate is welded to a part of the web only and leaves the bottom flange unsupported.

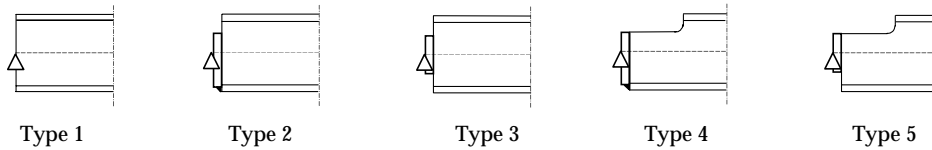


Figure 6: End conditions considered

Euler stability analyses and geometrically and physically non-linear calculations were carried out with the numerical models, so that it was possible to determine the relation between the reduction of the critical elastic buckling load and the reduction of the resistance due to the end condition.

Also, laboratory tests were carried out on (coped) beams with (partial) endplates. The test set-up was designed in such a way that rotations about the strong and weak axes and the translation in horizontal direction were free.

All six general criteria given above were not fully covered in this research.

- The combination of copes and fin plates or angles was not covered;
- The influence of partial restraints in real connections on buckling of coped beams was not taken into account;
- The research was limited to a uniformly distributed load and a concentrated load at mid-span;
- Because of problems with the load introduction in the test set-up, an accurate quantitative validation of the numerical models by these tests was not possible (see the Annex).

3 Description of the numerical models

The beams were modelled in the Finite Element Programme DIANA. Eight noded, curved shell elements were applied to model web and flanges. It was determined that four elements were needed to model each flange and also four elements to model the web. A problem with these elements is that they do not have a volume. Consequently, some differences exist between the geometric properties of the model and the geometric properties of the real cross-section. These differences remain small, except for the torsional constant I_t , as illustrated in table 1 by the example of an IPE 160 section. The relatively large difference in I_t is caused by the fact that the contribution of round-going stresses in the roots at the flange-web junctions are not simulated correctly in a model consisting of solely shell elements, as illustrated in figure 7.

Table 1: Geometric properties of a standard European IPE 160 section

Property	Model consisting of shells	Real section	Difference
A	1977 [mm ²]	2009 [mm ²]	1,62 %
I _y	8551391 [mm ⁴]	8692929 [mm ⁴]	1,63 %
I _z	681610 [mm ⁴]	681748 [mm ⁴]	0,02 %
I _{wa}	3959x10 ⁶ [mm ⁶]	3959x10 ⁶ [mm ⁶]	0,00 %
I _t	28511 [mm ⁴]	35406 [mm ⁴]	19,48 %

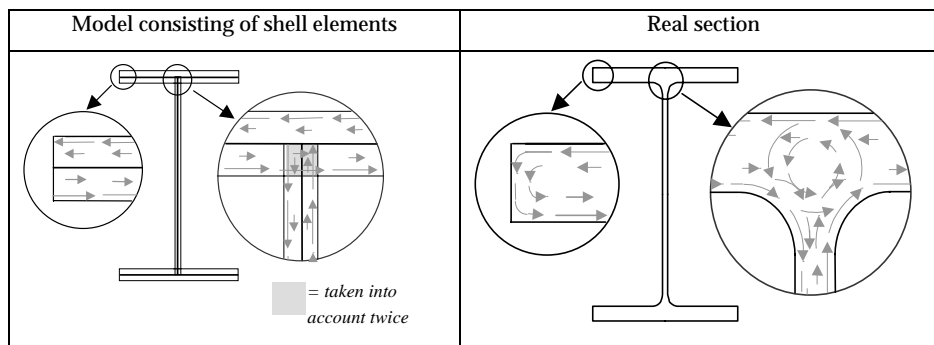


Figure 7: Difference in resistance to torsion between real section and model consisting of shell elements

Because the torsional constant is an important parameter for lateral-torsional buckling (see equation 1), a model consisting of solely shell elements gives a too low critical elastic buckling load. To obtain more accurate results, extra elements were added to the model. Beam elements were added at the flange-web junctions with a cross-section such that the total area of the model equals the area of the real beam. Torsional springs were added in the same points with a stiffness such that the total resistance against torsion of the model equals the torsional constant of the real section, see table 2 and figure 8. Equation (3) was used to determine the stiffness of the rotation spring element. As shown, the spring stiffness depends on the element length.

$$\begin{aligned}
 I_{t,tot} &= I_{t,shell} + 2 \cdot I_{t,spring} \\
 \frac{\varphi}{l} &= \frac{T}{GI_t} \\
 T &= k_{spring} \cdot \varphi \\
 k_{spring} &= \frac{GI_{t,spring}}{l}
 \end{aligned}
 \tag{3}$$

Table 2: Geometric properties of a modified model of an IPE 160 section

Property	Model (only shells)	Extra element (property per el.)	Model (shells and extra el.)	Real section	Difference
A	1977 [mm ²]	16 [mm ²]	2009 [mm ²]	2009 [mm ²]	0,00 %
I _y	8551391 [mm ⁴]	0 [mm ⁴]	8740776 [mm ⁴]	8692929 [mm ⁴]	0,55 %
I _z	681610 [mm ⁴]	68,8 [mm ⁴]	681748 [mm ⁴]	681748 [mm ⁴]	0,00 %
I _{wa}	3959x10 ⁶ [mm ⁶]	0 [mm ⁶]	3959x10 ⁶ [mm ⁶]	3959x10 ⁶ [mm ⁶]	0,00 %
I _t	28511 [mm ⁴]	r = 278,5 x 10 ⁶ /l [Nmm ² /mm rad]	35406 [mm ⁴]	35406 [mm ⁴]	0,00 %

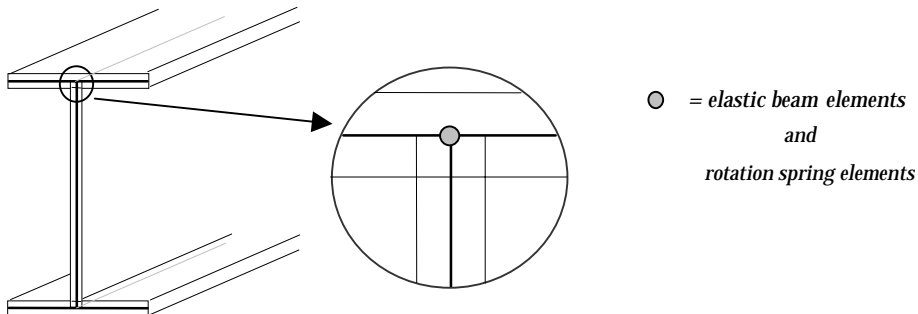


Figure 8: Model consisting of shell elements and beam elements and rotation springs in the roots

The elastic geometric properties of the model consisting of shells, beams and springs are almost equal to the properties of a real section. However, this does not apply for the plastic properties, as the extra elements only have elastic properties. To determine the influence of this, beam resistances

were also determined with models consisting of shells and extra elements that include a certain plastic limit. These models resulted in equal resistances as for models with extra elements without plasticity. The conclusion is that plasticity does not occur in the extra elements at loads equal to or lower than the buckling resistance. Therefore, in the numerical research, only elastic properties were applied for the extra elements.

To save computation time, only half the beam was modelled, with symmetry supports at mid-span. The symmetry supports consist of restraint against translation in longitudinal direction and restraints against rotations about the strong and weak axes.

In this case, it is permissible to model only one half of the beam to determine the resistance, as the first buckling mode is symmetric about mid-span and higher order buckling does not significantly influence the resistance.

The end conditions of figure 6 were modelled as follows:

- Fork supports (type 1) were modelled with stiff beam elements connected to the web and to the flanges of the beam end, preventing the distortion of the beam ends. The connections between these stiff beam elements were pinned, so that warping is free, see figure 9. As the translation in longitudinal direction is already restrained at mid-span, this translation is free at the end of the beam. Constraints are applied to translations in direction of the strong and weak axes and to rotation about the longitudinal axis at the end of the beam (simple supports).
- Endplate (type 2 and type 3) connections were modelled with beam elements with such stiffness that the elastic properties of the beam elements are equal to the elastic properties of the real endplate. The connections between the beam elements were rigid, contrary to type 1 connections. A beam element in longitudinal direction was applied to model the endplate thickness. For the part of the web not supported by the endplate, mesh refinement was applied in order to allow for local web buckling see figure 10. In this region, 7 integration points through thickness were applied instead of three.
- For coped connections (type 4 and type 5), mesh refinement was used for that part of the web where local buckling is to be expected, see figure 11. In these regions, seven integration points through thickness were applied.

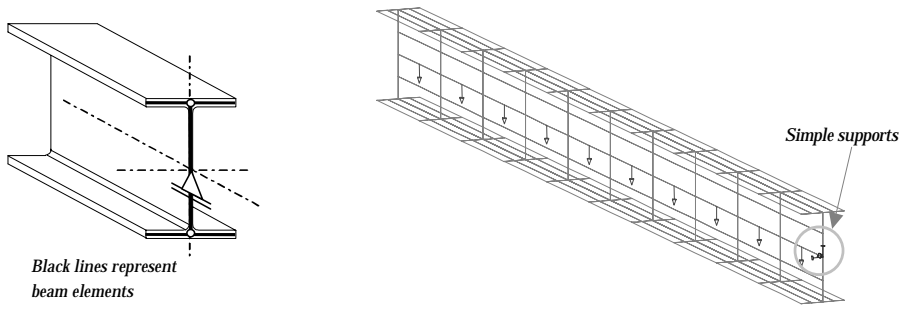


Figure 9: Model of a beam with type 1 connection

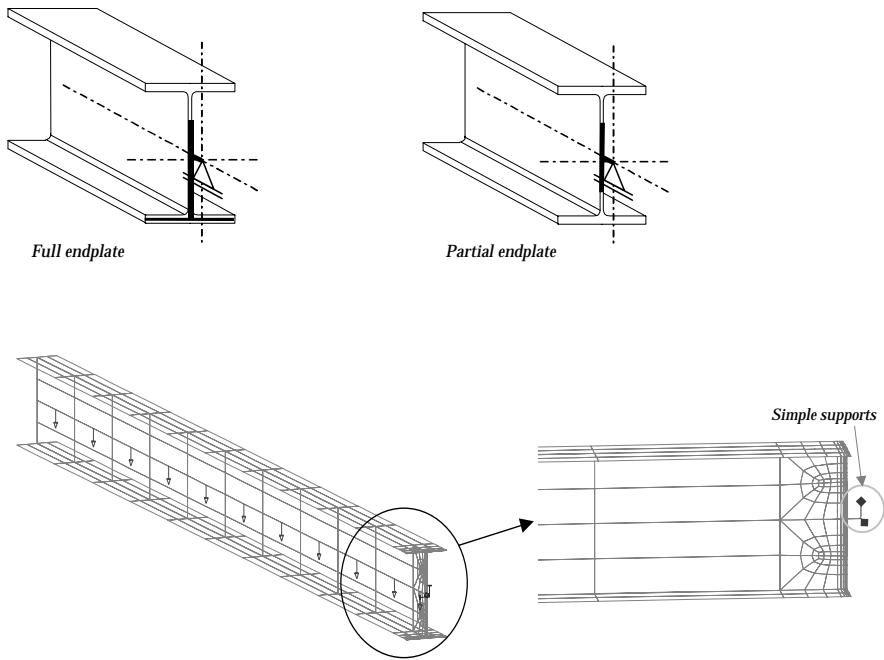


Figure 10: Models of beams with type 2 and type 3 connections

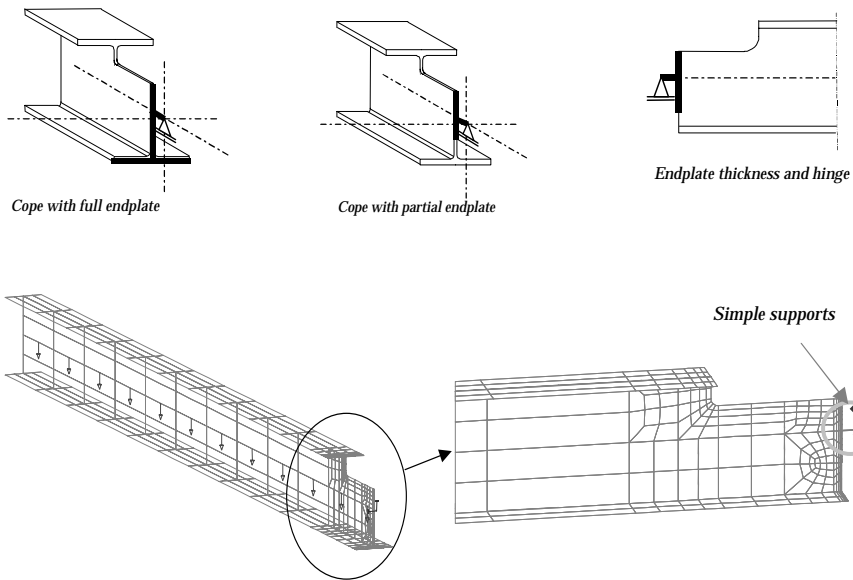


Figure 11: Models of beams with type 4 and type 5 connections

The Von Mises yield criterion was used to describe plasticity. The stress-strain relation according to the Dutch code NEN 6770 (20) was applied (see figure 12). Work hardening was included. Initial stresses as given in prEN 1993-1-1 (19) were applied in the models (see figure 13).

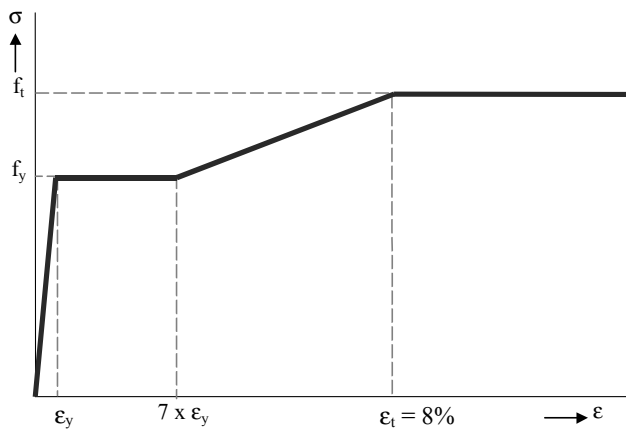


Figure 12: Stress-to-strain relation according to NEN 6770

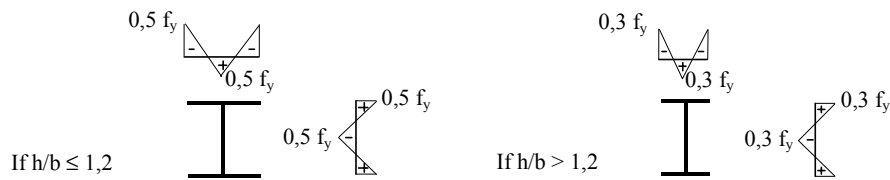


Figure 13: Residual normal stresses in I-sections according to prEN 1993-1-1

4 Validation of numerical models

The numerical models were validated in four steps.

4.1 First validation step

The first validation step consisted of a comparison between analytically derived values for deformations, stresses and critical elastic buckling loads and values determined with the numerical models. For this purpose, two structures were considered.

The first structure is the simply supported, laterally unrestrained beam loaded in bending about the strong axis, for which equation (1) has been derived. Three models were made: one of a relatively stocky beam for which restrained warping gives the highest contribution to the resistance against lateral-torsional buckling, one of a relatively slender beam for which torsion gives the highest contribution to the resistance against buckling and one of a beam for which the contributions of torsion and restrained warping are almost equal.

Linear elastic displacements and normal stresses determined with the models were equal to analytical solutions. The numerical models resulted in critical elastic buckling loads approximately 2 % lower than the analytical solution. The difference between the analytical solution and the numerically determined value is possibly caused by the influence of local deformations in the compressed upper flange and the web, which is taken into account in the DIANA calculation, but not in the analytical model for the critical elastic lateral-torsional buckling load.

The second structure is the coped part (T-part) of a beam, loaded in torsion. Rotation about the longitudinal axis was restrained at the support, while warping and transverse contraction were not restrained at the support, see figure 14. The analytical equation for the linear elastic relation between load and deformation is given in equation (3). The numerically determined rotation was 0,8% lower than the analytical value.

From results of the first validation step it was concluded that warping and torsion is sufficiently accurately described by the models. Also, simple supports and standard conditions of restraint were modelled properly.

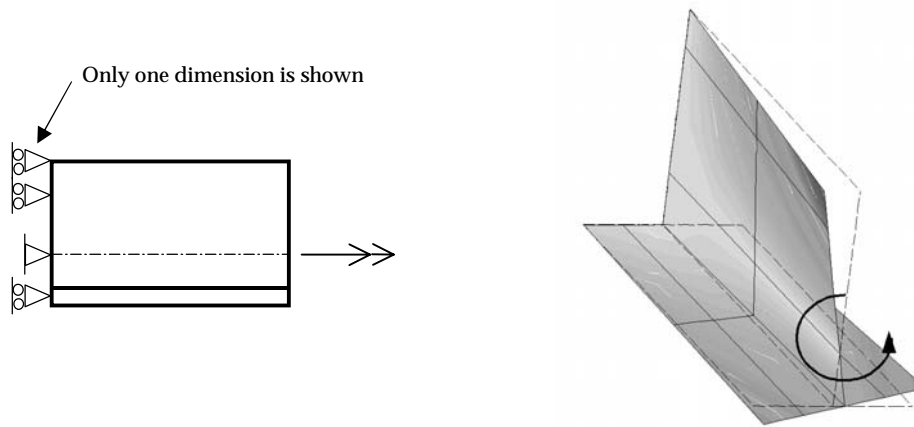


Figure 14: Second structure of first validation step: torsion on coped section

4.2 Second validation step

In the first validation step, only results of linear elastic and Euler buckling analyses could be checked. In the second validation step, non-linear analyses were checked. The second validation step consisted of a comparison between numerically determined beam resistances and buckling curve 'a' of prEN 1993-1-1 (19). This curve is based on extensive research with tests and some numerical models and is therefore considered as rather accurate. As the curve is used for all European sections, it should be an upper bound for a specific section.

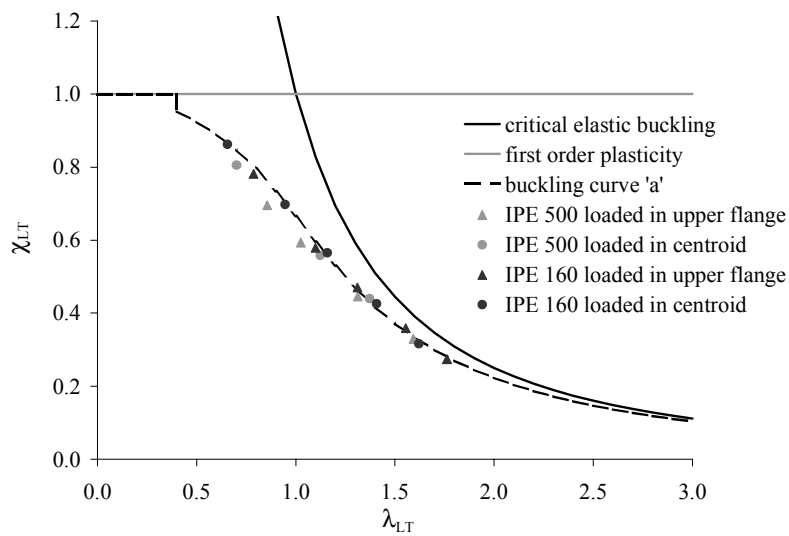


Figure 15: 2nd validation step: comparison of numerical buckling resistance with prEN 1993-1-1

For this validation step, models were made of IPE 160 and IPE 500 beams with various values for the slenderness (various spans). The applied initial geometric imperfection had the same shape as the first critical elastic buckling mode. The maximum amplitude of this initial imperfection was taken as 0,001 times the span. The value of the yield stress was taken as 235 N/mm².

The dots in figure 15 show the results of the numerical simulations. The numerically determined relation between relative slenderness and buckling resistance of the considered beams follow the buckling curve 'a' of prEN 1993-1-1 quite well. Only the numerically determined buckling resistances of stocky IPE 500 beams are slightly lower than indicated by buckling curve 'a', but differences remain small.

4.3 Third validation step

The third validation step consisted of a comparison with other numerical models. For a proper comparison, these other models should also include the section roots.

Results were compared with two other numerical models representing a simply supported uniform beam with type 1 connections.

The first model was developed and described by Greiner, Salzgeber and Offner, 2000 (6) and consisted of 100 open-section beam elements, including warping and torsion with 17 integration points for the web and 17 integration points for each flange. The used Finite Element Programme was ABAQUS.

The geometric imperfection in the model of Greiner et al., 2000 (6) was defined by an initial bow imperfection of parabolic shape in the lateral direction with amplitude $L/1000$, while in the current research, the first elastic buckling mode was scaled so that the amplitude in lateral direction was equal to $L/1000$. The amplitude was therefore equal, but the mode was slightly different.

Instead of the linear distribution of the residual stresses (figure 13), Greiner et al., 2000 (6) used a parabolic distribution.

Both the critical elastic buckling load and the beam resistance were compared for a relatively slender and a relatively stocky beam. The considered load cases were a constant moment, a uniformly distributed load and a concentrated load at mid-span. In all six cases, the elastic critical buckling loads obtained by the models were equal. In case of constant moment loading, the beam resistance was equal as well. However, in case of loading by a concentrated load or a uniformly distributed load, the model used in the current research resulted in resistances respectively up to 10% and up to 6% lower than predicted by the model of Greiner et al., 2000 (6).

Loading by a uniformly distributed load or a concentrated load results in shear stresses and shear deformations. Local (web) deformations can be larger than in case of a constant moment loading. These effects are taken into account in the models used in the current research, but possibly not in the elements used in the models developed by Greiner et. al. A coped beam has no uniform cross-

section along its span and it is therefore not possible to accurately model a coped beam with the elements used by Greiner et al., 2000 (6).

The second model is a model consisting of solid elements, see figure 16. The model was also developed in the current research in the Finite Element Programme DIANA. Initial imperfections, load conditions and support conditions were the same as in case of the model consisting of shell elements. Both the critical elastic buckling load and the beam resistance resulting from the different models were compared for a relatively slender and a relatively stocky beam loaded by a constant moment, a uniformly distributed load and a concentrated load applied at mid-span. The model consisting of solid elements resulted in a critical elastic buckling load that was up to 0,5% higher and a resistance that was up to 2,2% higher than in case of the model consisting of shell elements.

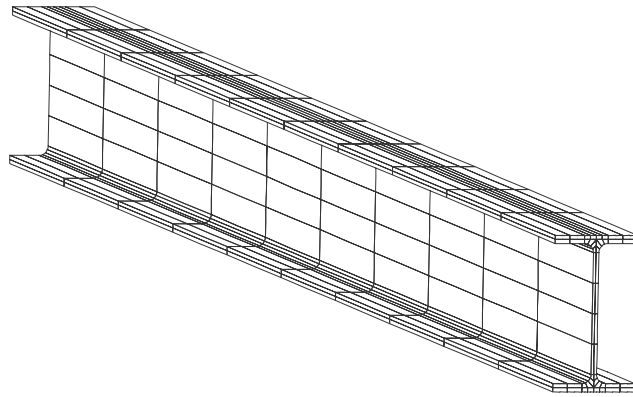


Figure 16: Model consisting of solid elements

The third validation step shows that the differences in buckling resistance between the model consisting of shell elements and the model consisting of solid elements are small. The maximum differences in buckling resistance between the model consisting of shell elements and the model consisting of beam elements developed by Greiner et al., 2000 (6) are larger, but the differences remain small for most beams considered. A possible explanation is given for the differences. The critical elastic buckling loads of the three models were almost equal.

In order to save computation time, the model consisting of shell elements is used in this study instead of the model consisting of solid elements.

4.4 Fourth validation step

The fourth validation step was planned for a further validation of the numerical models for beams with the five connections considered. For this validation step a series of tests was carried out. However, because of problems with the load introduction, the tested beams could not exactly be simulated with numerical models. Only a global comparison between buckling resistances was

possible. This comparison showed that the numerically determined resistances were comparable with the resistances determined with the tests. The tests and the comparison are briefly described in the Annex to this paper. For a complete description, see Maljaars, 2001 (13) and Maljaars et al., 2002a (21).

Although this fourth validation step was not fully successfully completed, the results of the three first validation steps were considered to give sufficient confidence in the models. On that basis it was decided to use these models for a parameter study.

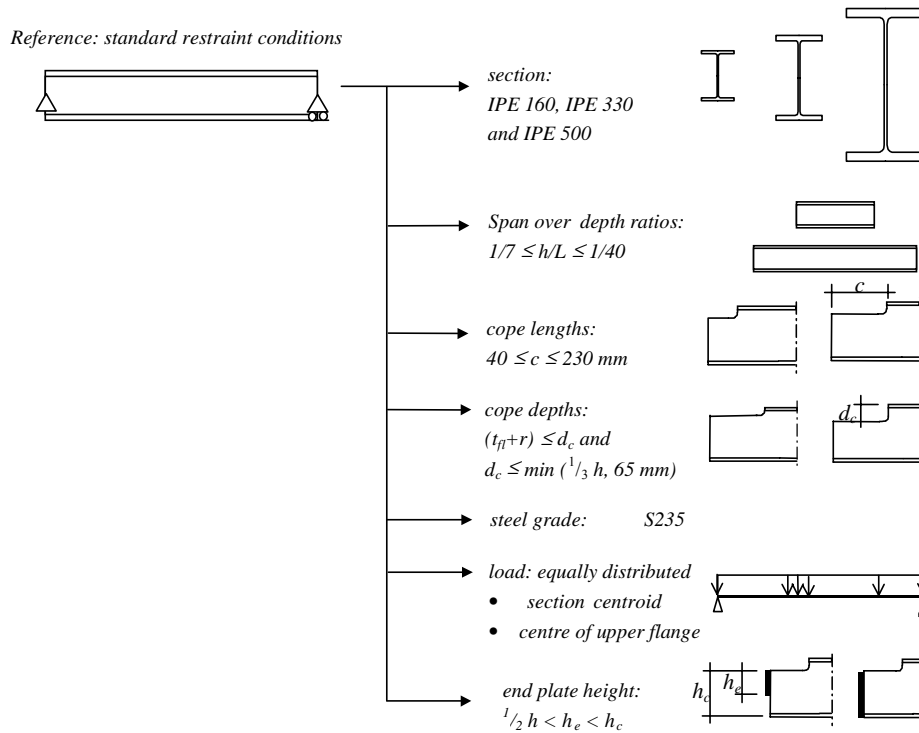


Figure 17: Parameter field of the parameter study

5 Parameter study to the influence of type 2 to type 5 connections on buckling of beams

A parameter study was carried out with the numerical models, in order to quantify the influence of endplates and copes on the beam resistance. In this research, the critical elastic buckling load and the resistance of a beam with type 2 to type 5 connections was compared with the critical elastic buckling load and the resistance of a reference beam with the same physical and geometrical properties, but with type 1 connections, for which most codes for steel structures give verification rules. Calculations were carried out for standard European IPE beams with various spans and

various dimensions of endplates and copes. All beams were simply supported. The parameter field is described in figure 17.

The results of the calculations are shortly discussed in this paper. A more extensive discussion of results is given in Maljaars, 2001 (13) and Maljaars et al., 2002b (22).

In this paper, the influence of the connection type on the critical elastic buckling load is discussed first. Following, the relation with the beam resistance is presented.

5.1 Reduction of the critical elastic buckling load for type 2 and type 3 connections

In figure 18, results are plotted of some calculations for IPE160 beams loaded in the centre of the upper flange. The vertical axis gives the critical elastic buckling load of the beam with end plates (type 2 or type 3) as a percentage of the critical elastic buckling load of the reference beam (type 1). The reduction in critical load due to the endplate is significant for very short beams, but the influence of the endplate decreases for increasing spans. For spans most applied in practice ($L/h > 25$), the reduction in critical load is 12% maximum, in case of very short endplates.

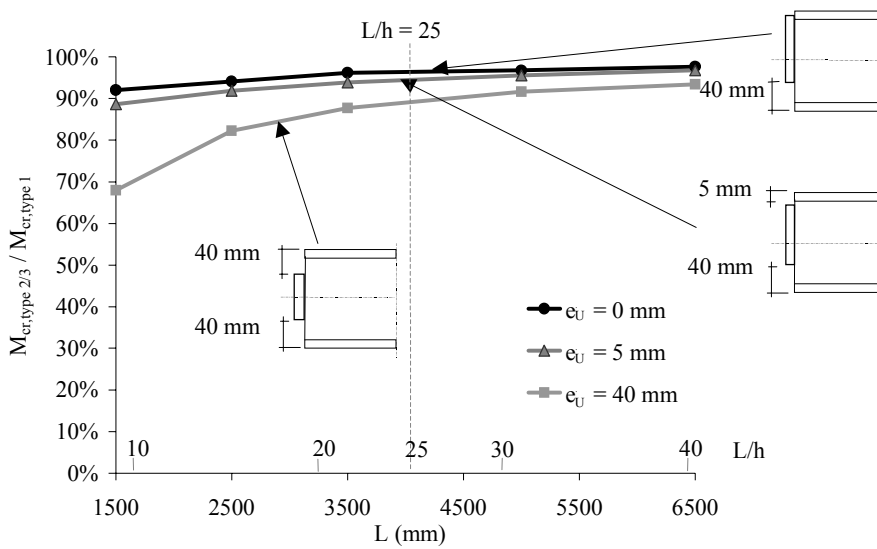


Figure 18: Endplate influence on critical load as a function of span on IPE160 beams

In figure 19, results are plotted of calculations with short IPE 500 beams with a span of 3500 mm ($L/h = 7$) and with type 2 and type 3 connections. The unsupported web height above the endplate (e_u) is shown on the horizontal axis, while the different lines refer to endplates with different values of the unsupported web height under the end plate (e_b).

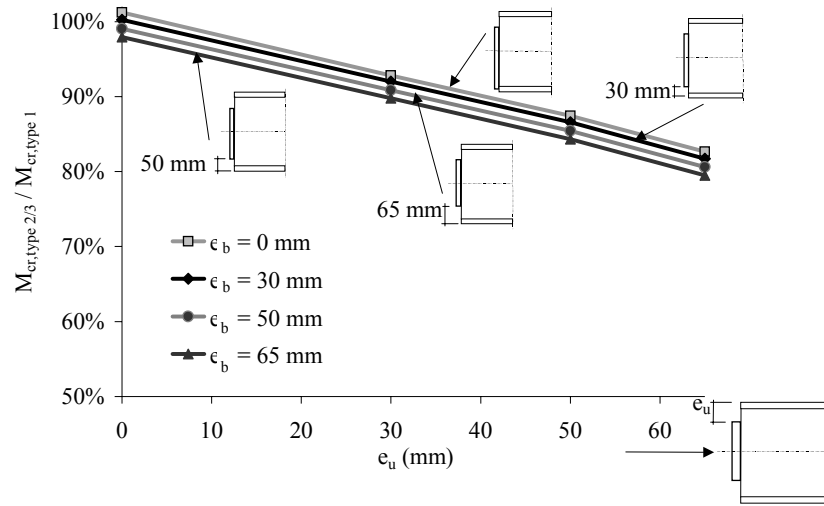


Figure 19: Critical load as a function of unsupported web height from top flange

The different lines are closely together, indicating that for beams with uniform cross-section, leaving the bottom flange unsupported results in just a small reduction of the critical load. In contrary, the influence of e_u is significant. The relation between the reduction in critical load and e_u is approximately linear.

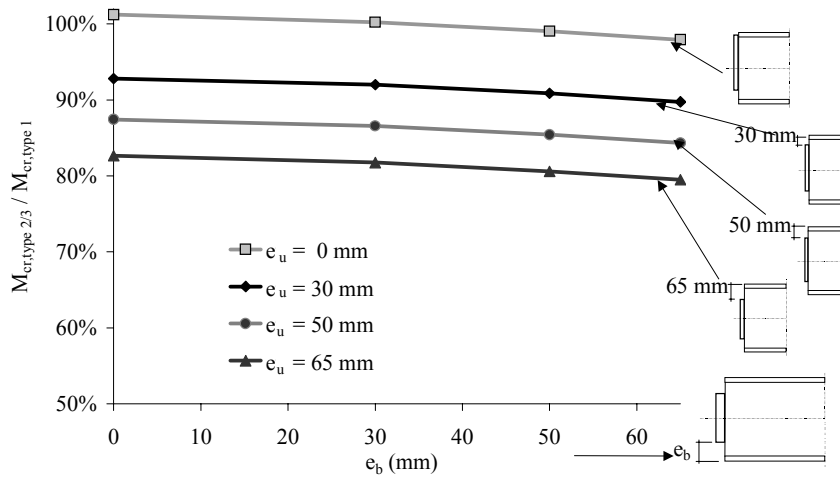


Figure 20: Critical load as a function of unsupported web height from bottom flange

In figure 20, the same data is plotted as in figure 19. In figure 20 however, e_b is plotted on the horizontal axis and e_u is indicated by different lines. The relation between the critical load reduction and e_b is approximately linear, however the reduction with increasing e_b is limited.

In total, 155 beams with type 2 and type 3 connections were analysed. The reduction of the critical load due to the endplate can be determined with equation (4). This equation is based on curve fitting of the numerical results. The symbols are explained in figure 21.

$$M_{cr;type2/type3} = \alpha \cdot M_{cr;type1} \quad (4)$$

$$\alpha = 1 - A_1 \frac{e_u}{h} \left(\frac{h}{L}\right)^{A_2} - A_3 \frac{e_b}{h} \left(\frac{h}{L}\right)^{A_4}$$

For loads applied in the centre of the upper flange, the constants A1 –A4 are:

$$A_1 = 22,7 \quad A_3 = 0,875$$

$$A_2 = 1,44 \quad A_4 = 0,450$$

For loads applied in the section centroid, the constants A1 –A4 are:

$$A_1 = 9,93 \quad A_3 = 1,28$$

$$A_2 = 1,10 \quad A_4 = 0,860$$

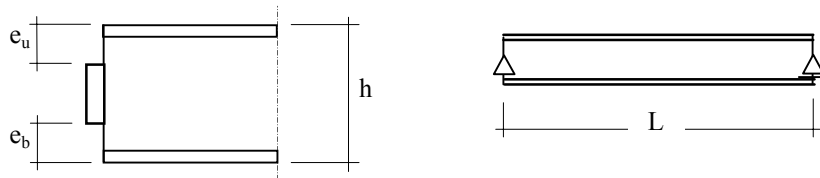


Figure 21: Symbols used in equation (4)

5.2 Reduction of the critical elastic buckling load for type 4 connections

In figure 22, the results are plotted for some IPE 160 beams with type 4 connections. The span is shown on the horizontal axis and different lines indicate various cope lengths (c). The cope depth (d_c) was 40 mm. The influence of copes is greater for smaller spans. This is the case for cope lengths as well as for cope depths. The maximum reduction of the critical load is 75% for short spans to 20% for commonly applied span over depth ratios ($L/h = 25$).

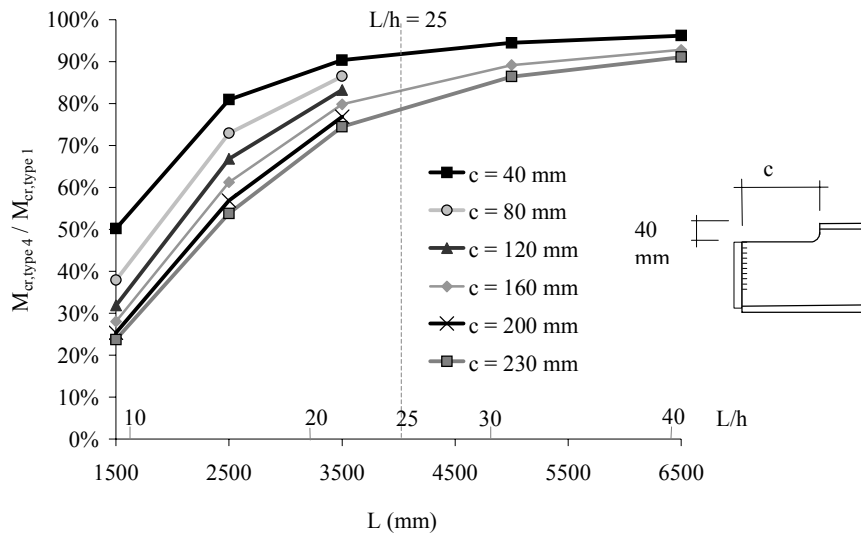


Figure 22: Reduction in critical load due to cope length for beams with type 4 connections with various spans

In figure 23, results are plotted for short IPE 160 beams with a span of 1500 mm ($L/h = 9$) and type 4 connections. Parameter c is shown on the horizontal axis and different lines indicate values for d_c . The influence of d_c is greater for smaller cope lengths. The relation between cope length and reduction in critical elastic buckling load is non-linear.

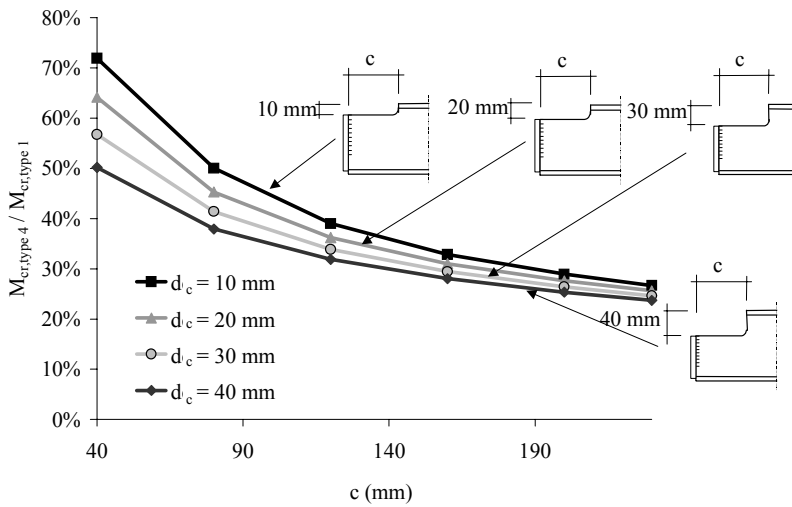


Figure 23: Reduction in critical load as a function of cope length for type 4 connections

In figure 24, the same data is plotted as in figure 23 but this time, the cope depth (d_c) is plotted on the horizontal axis, while the different lines indicate various cope lengths (c). The relation between reduction in critical load and cope depth (d_c) is approximately linear.

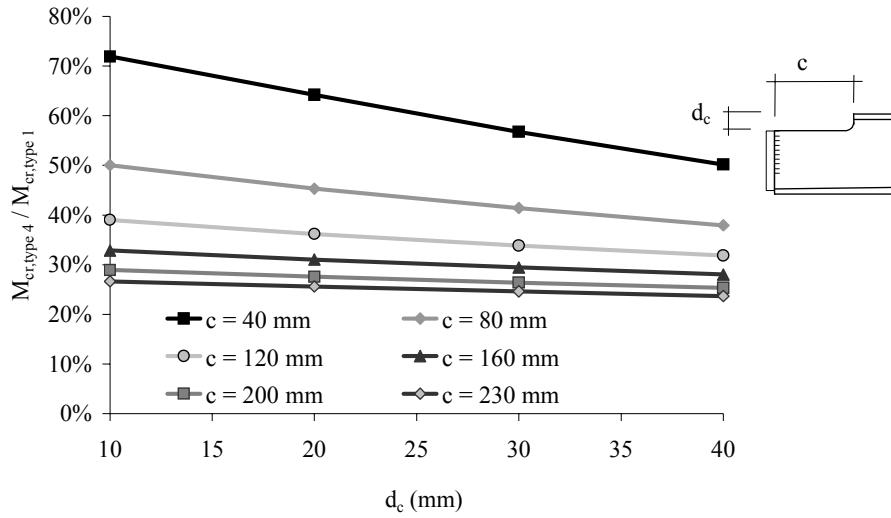


Figure 24: Reduction in critical load as a function of cope depth

In total, 131 beams with type 4 connections were analysed. The reduction of the critical load due to the cope can be determined with equation (5). Again, the equation is based on curve fitting of the numerical results. The symbols are explained in figure 25.

$$M_{cr,type 4} = \alpha \cdot M_{cr,type 1}$$

$$\alpha = 1 - B_1 \frac{d_c}{c} \left(\frac{h}{L} \right)^{B_2} - (B_3)^{B_4} \left(\frac{h}{L} \right)^{B_5} \quad (5)$$

$$B_3 = B_6 \left(\frac{c}{h} - B_7 \right) \text{ and } B_3 \geq 0$$

In case the load is applied in the centre of the upper flange:

$$B_1 = 22,8 \quad B_4 = 0,344 \quad B_6 = 4457$$

$$B_2 = 1,89 \quad B_5 = 1,44 \quad B_7 = 0,229$$

In case the load is applied in the section centroid:

$$B_1 = 23,3 \quad B_4 = 0,361 \quad B_6 = 7671$$

$$B_2 = 1,97 \quad B_5 = 1,58 \quad B_7 = 0,236$$

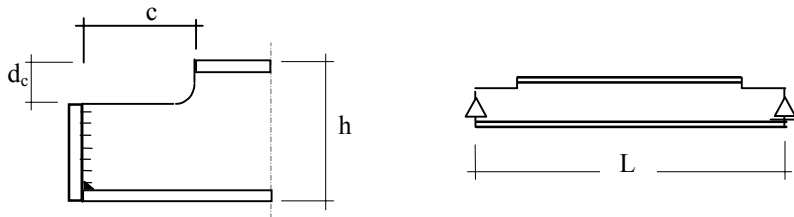


Figure 25: Symbols used in equation (5)

5.3 Reduction of the critical elastic buckling load for type 5 connections

In figure 26, results are plotted of some IPE 160 beams with type 5 connections. The span is shown on the horizontal axis and different lines indicate various cope lengths. All beams have a very short end plate, which leaves 40 mm of the web unsupported. The figure shows that the influence of copes is greater for smaller spans, as was the case for type 4 connections. The maximum reduction of the critical load is 85% for short spans to 40% for commonly applied span to depth ratios ($L/h = 25$).

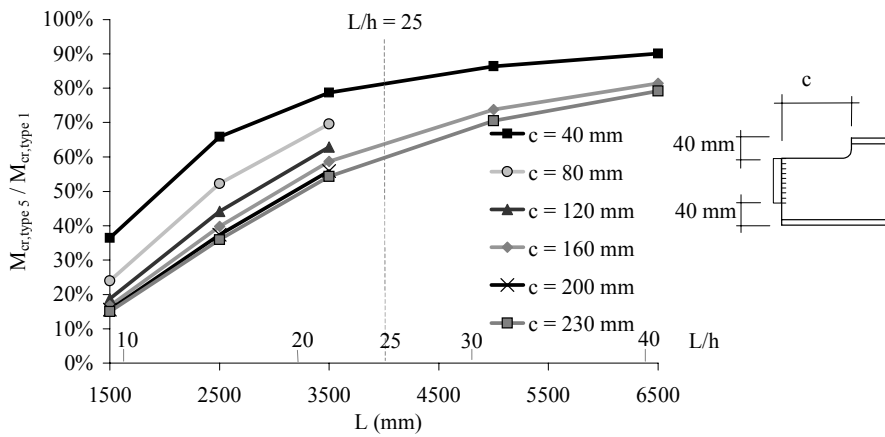


Figure 26: Reduction in critical load due to cope length for beams with type 5 connections and various spans

In figure 27, results are plotted for IPE160 sections with type 5 connections with cope dimensions $c = 230$ mm and $d_c = 40$ mm. The different lines represent different endplate heights. As in figure 26, the span is shown on the horizontal axis. The beams have a large cope length of 230 mm. Contrary to type 2 connections, the influence of e_b is significant for type 5 connections.

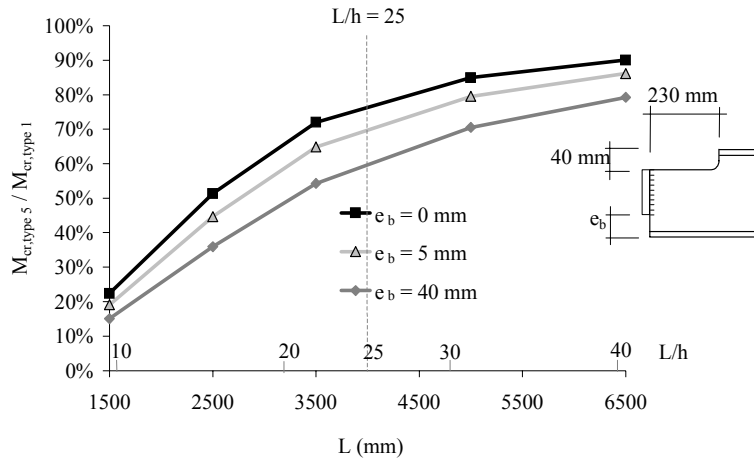


Figure 27: Reduction in critical load due to endplate height for beams with type 4 connections with various spans

In figure 28, results are plotted for short IPE 160 beams with a span of 1500 mm ($L/h = 9$) and with type 5 connections. Different values for c are shown on the horizontal axis and different lines indicate various values for e_b . The relation between cope length and reduction in critical elastic buckling load is non-linear.

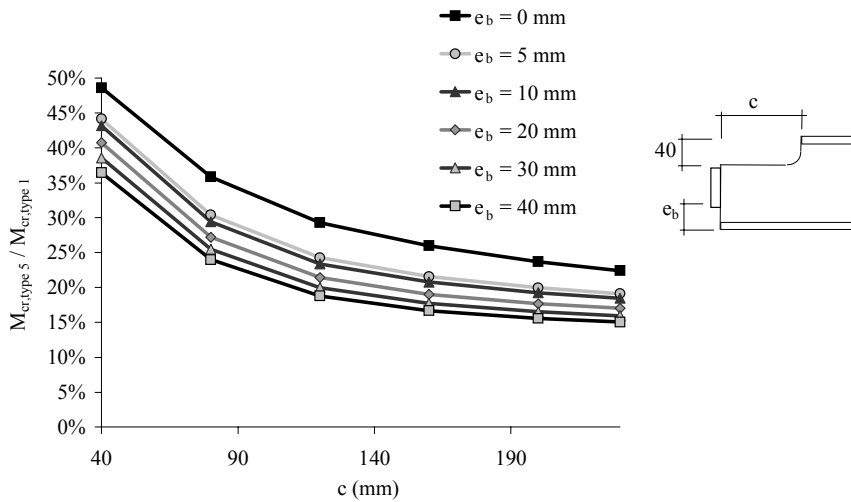


Figure 28: Reduction in critical load as a function of cope length for type 5 connections (IPE160, span 1500 mm)

In figure 29, the same data is plotted as in figure 28, but now e_b is plotted on the horizontal axis and the different lines represent different values of c . The relation between the critical load reduction and e_b is approximately linear, except for the case that the endplate covers (almost) the total web but not the bottom flange ($e_b=0$). In this case, the web supplies sufficient support to the bottom flange to prevent it from buckling, although the bottom flange is not welded to the endplate.

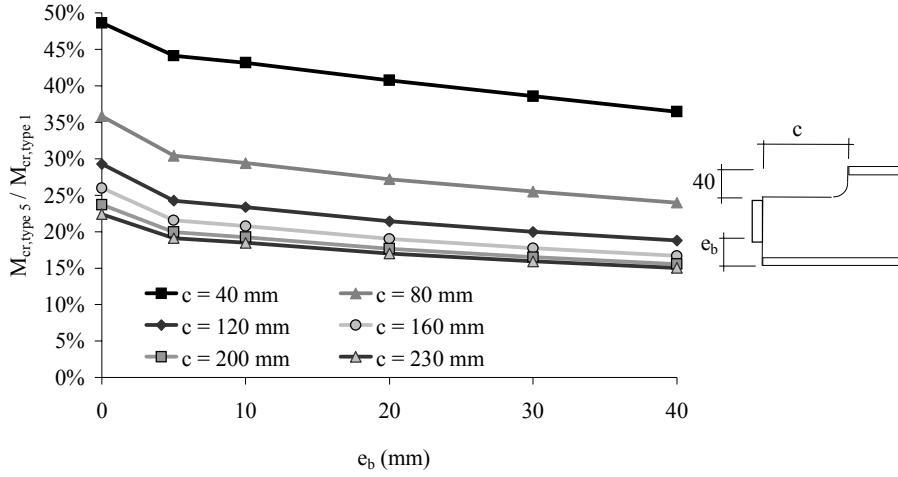


Figure 29: Reduction in critical load as a function of endplate height for type 5 connections (IPE 160, span 1500 mm)

Type 5 connections with $e_b = 0$ can be calculated as type 4 connections. The critical load of other type 5 connections can be determined with equation (6). This equation is based on 300 FEM calculations of beams with type 5 connections. Symbols are explained in figure 30.

$$M_{cr,type 5} = \alpha \cdot M_{cr,type 1}$$

$$\alpha = 1 - D_1 \frac{d_c}{c} \left(\frac{h}{L}\right)^{D_2} - (D_3)^{D_4} \left(\frac{h}{L}\right)^{D_5} - D_8 \frac{e}{h} \left(\frac{h}{L}\right)^{D_9} \quad (6)$$

$$D_3 = D_6 \left(\frac{c}{h} - D_7\right) \text{ and } D_3 > 0$$

In case of a distributed load applied in the centre of the upper flange:

$$D_1 = 21,5 \quad D_4 = 0,288 \quad D_6 = 1149 \quad D_8 = 1,01$$

$$D_2 = 1,81 \quad D_5 = 1,04 \quad D_7 = 0,239 \quad D_9 = 0,479$$

In case of a distributed load applied in the section centroid:

$$D_1 = 21,6 \quad D_4 = 0,322 \quad D_6 = 1883 \quad D_8 = 0,709$$

$$D_2 = 1,83 \quad D_5 = 1,21 \quad D_7 = 0,244 \quad D_9 = 0,419$$

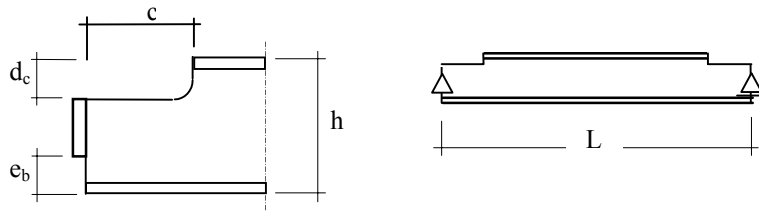


Figure 30: Symbols used in equation (6)

The mean values and the standard deviations of the ratio between the critical elastic buckling load according to equations (4) to (6) and the numerically determined critical elastic buckling load is given in table 3. The mean values are just below one, which is on the safe side.

Table 3: Mean value and standard deviation of quotient ($M_{cr, equation}/M_{cr, numerical}$)

Connection	Load application	Mean value (μ)	Standard deviation (σ)
Types 2 and 3	Upper flange	0,96	0,029
	Centroid	0,92	0,032
Type 4	Upper flange	0,89	0,061
	Centroid	0,89	0,064
Type 5	Upper flange	0,87	0,085
	Centroid	0,83	0,096

5.4 Reduction of the beam resistance

In the previous paragraph, the reduction in critical elastic buckling load was quantified. In this paragraph, a method is presented for determining the beam resistance .

The beam resistance relative to the plastic capacity and the critical elastic buckling loads are plotted in figure 31. Each dot represents a specific beam with type 2, 3, 4 or 5 connections. The relative slenderness and the relative resistance was determined using the critical elastic buckling load and the buckling resistance according to the finite element simulations of each beam. Buckling curve 'a', which provides correct resistances in case of type 1 connections, is not always safe for the other connections. This is caused by the fact that yielding occurs in the coped region or in the unsupported part of the web.

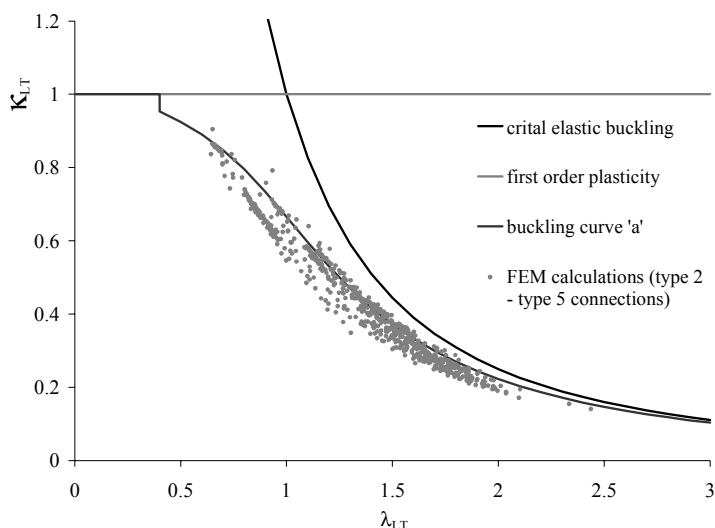


Figure 31: Critical elastic buckling loads and beam resistances for beams with type 2 to type 5 connections

A better fit can be obtained by the use of alternative buckling curves. The choice of the buckling curves depends on the type of connection and on the reduction of the critical elastic buckling load. This reduction is given by factor α , determined with equation 4, 5 or 6.

- For type 2 and type 3 connections, the following buckling curve should be used
 - Buckling curve 'b' when $0,85 \leq \alpha < 1,0$
 - Buckling curve 'c' when $\alpha < 0,85$
- For type 4 connections, buckling curve 'b' should be used, independent of α .
- For type 5 connections the following buckling curve should be used.
 - Buckling curve 'b' when $0,70 \leq \alpha < 1,0$
 - Buckling curve 'c' when $0,50 \leq \alpha < 0,70$
 - Buckling curve 'd' when $\alpha < 0,50$

The proposed verification method for buckling of beams with copes and / or partial endplates thus consists of the following steps:

- Factor α may be determined using equations 4 to 6
- The relative slenderness may be determined using $M_{cr} = \alpha \cdot M_{cr,type 1}$
- The appropriate buckling curve may be chosen based on the type of connection and the value for α .
- The buckling resistance relative to the plastic capacity, χ_{LT} , may be determined with the relative slenderness and the appropriate buckling curve.

The accuracy of this proposed verification method is shown in figure 32 for type 2 and type 3 connections, in figure 33 for type 4 connections and in figure 34 for type 5 connections. In these figures, the buckling factor determined with the verification method described above, $\chi_{LT,vm}$, on the vertical axis is compared with the numerically determined buckling factor $\chi_{LT,num}$ on the horizontal axis. The buckling factor $\chi_{LT,num}$ is defined as the numerically determined resistance divided by the plastic capacity.

The figures also give the mean value and the standard deviation of the ratio between $\chi_{LT,vm}$ and $\chi_{LT,num}$. The mean values of this ratio are below one, which means that the procedure proposed is on the safe side.

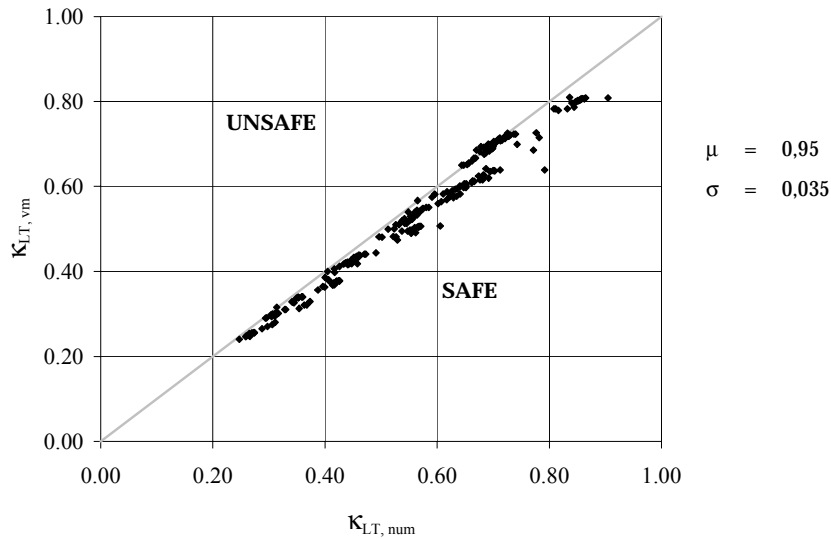


Figure 32: Comparison of beam resistances between numerical model and proposed verification method for type 2 and type 3 connections

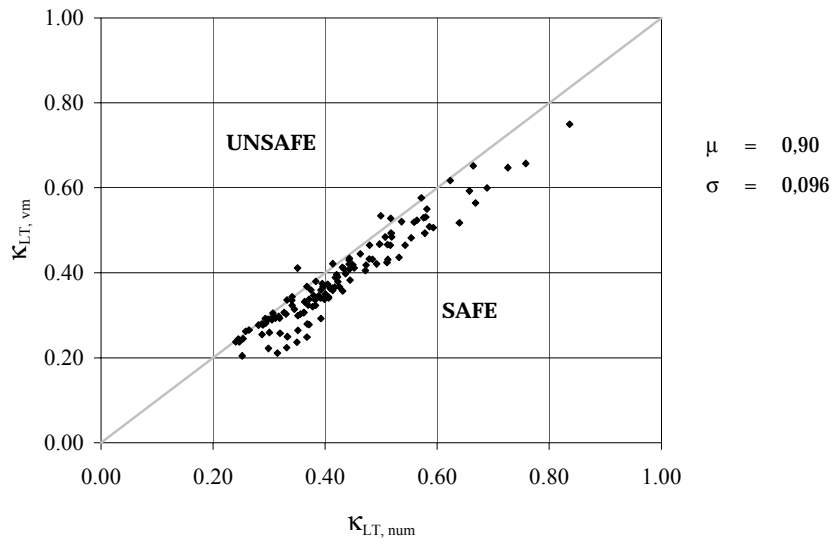


Figure 33: Comparison of beam resistances between numerical model and proposed verification method for type 4 connections

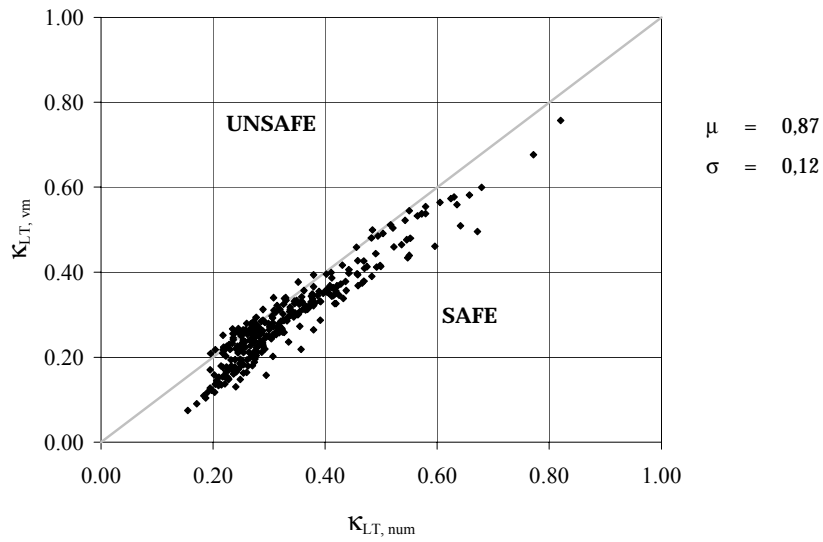


Figure 34: Comparison of beam resistances between numerical model and proposed verification method for type 5 connections

6 Conclusions and recommendations

Conclusions:

- Lateral-torsional buckling and local web buckling of I-sections can be modelled with the Finite Element Method;
- Copes and partial end plates reduce the elastic critical buckling load. The influence of copes and end plates is particularly significant for beams with relatively small span to depth ratios;
- A combination of a cope and a partial endplate that leaves the bottom flange unsupported leads to the greatest reduction in the critical elastic buckling load and in the beam resistance;
- For beams with copes and / or partial endplates with a certain relative slenderness, the reduction of the plastic capacity is larger than for beams with the same relative slenderness but supported by forks and having uniform cross-section, so the use of the same buckling curve for these beams is not applicable.
- The post buckling behaviour of beams with copes and partial endplates is worse than of beams with fork supports.

Recommendations:

- The equations proposed for the critical elastic buckling load of beams with copes and / or endplates are derived with a curve fitting method. Strictly speaking these equations are only applicable within the range of parameters used in the parameter study. It is recommended to develop an analytical method for buckling of coped beams.
- The proposed use of alternative buckling curves to determine the resistance does not always satisfactory correspond to the numerically determined resistance. For a better determination of the buckling resistance, it is recommended that yielding of the web be studied analytically for beams with copes and / or endplates;
- The critical elastic buckling load and the beam resistance of coped beams loaded by other loads than a uniformly distributed load should be determined;
- The critical elastic buckling load and the beam resistance of coped beams in combination with angles and fin plates should be determined.
- The application of beams with copes in combination with partial endplates is not recommended because these beams show the largest reduction in beam resistance and post buckling behaviour.
- The test set-up described in the Annex should be further improved so that the tests planned for the fourth validation step can reliably be carried out.

References

- Abspoel, R., J.W.B. Stark. *Elastic lateral buckling of coped beams*. Proceedings of Eurosteel 1999, Prague, Elsevier 1999.
- Abspoel, R., J.W.B. Stark. *Elastic lateral buckling of coped beams*. Stability and Ductility of Steel Structures, Proceedings of the 6th International Colloquium 1999, Timisoara, Elsevier 1999.
- Cheng, J.J.R., J.A. Yura. *Lateral Buckling Test on Coped Steel Beams*. Journal of Structural Engineering, ASCE, 1988, 114 (1), p. 16-30.
- Cheng, J.J.R., J.A. Yura, C.P. Johnson. *Lateral Buckling of Coped Steel Beams*. Journal of Structural Engineering, ASCE, 1988, 114 (1), p. 1-15.
- Du Plessis, D.P. *Lateral-torsional Buckling of End Notched Steel Beams*. Proceedings, International Colloquium on Stability of Structures under Static and Dynamic Loads, ASCE, Washington D.C., 1977.
- Greiner, R., G. Salzgeber, R. Ofner. *New lateral-torsional buckling curves κ_{LT} – numerical simulations and design formulae*. ECCS TC 8 –Report 30th June 2000.
- Lam, C.C., M.C.H. Yam, V.P. Iu, J.J.R. Cheng. *Design for lateral-torsional buckling of coped I-beams*. Journal of Constructional Steel Research 54, p 423-443, Elsevier 2000.
- Lindner, J., R. Gietzelt. *Zur Tragfähigkeit ausgeklinkter Träger*. Stahlbau, 1985.
- Lindner, J. *Influence of constructional details on the load carrying capacity of beams*. Engineering structures, 1996, 18 (10), p. 752-758.
- Lindner, J. *Influence of Structural Connecting Details on the Load Carrying Capacity of Beams*, Internationale Vereinigung für Brückenbau und Hochbau, 13th congress Helsinki, 1988.
- Lindner, J., R. Gietzelt. *Biegedrillknicklasten von Walzprofilen IPE200 und IPE160 mit angeschweißten Kopfplatten und baupraktischen Ausklinkungen an den Trägerenden*. Vr 2042, Technische Universität Berlin, 1982.
- Lindner, J. *Einfluss von Quer-einspannungen auf die Gabellagerung*. Vr 2065, Technische Universität Berlin, 1987.
- Lindner, J. *Biegedrillknickuntersuchungen an ausgeklinkten Trägern unter Berücksichtigung der Quereinspannung*. Vr 2073, Technische Universität Berlin, 1985.
- Maljaars, J. Thesis report *Lateral-torsional buckling of coped girders*. Delft University of Technology, May 2001.
- Maljaars, J., J.W.B. Stark, H.M.R.M. Steenbergen and R. Abspoel. *Numerical simulation of lateral-torsional buckling of coped girders*, 15th ASCE Engineering Mechanics Conference – Stability Research, New York, USA, June 2-5 2002a.
- Maljaars, J., J.W.B. Stark, H.M.R.M. Steenbergen and R. Abspoel. *Lateral-torsional buckling capacities of coped girders*, European Conference on Steel Structures, Coimbra, Portugal, September 19-20 2002b.

- NEN 6770: 1997 TGB 1990 – Steel Structures – Basic requirements and basic rules for calculation of predominantly statically loaded structures.
- Pi, Y.-L., N.S. Trahair. *Distortion and Warping at Beam Supports*. Journal of Structural Engineering, ASCE, 2000, 126 (11), p. 1279-128
- prEN 1993-1-1, Eurocode 3: Design of Steel Structures – part 1-1: General rules and rules for buildings.
- Timoshenko, S.P. and J.M. Gere. *Theory of elastic stability*. 2nd edition, McGraw-Hill Book Company, 1961.
- Trahair, N.S. *Flexural-Torsional Buckling of Structures*. 1st edition, E & FN Spon (Chapmann and Hall), 1993.
- Vacharajittiphan, P., N.S. Trahair. *Warping and distortion at I-section joints*. Journal of Structural Div., ASCE, 1974, 100 (3), p. 547-564.

Symbols used

- α = Reduction factor for the critical elastic buckling load due to the cope and / or the endplate
- φ = Rotation angle between first node and second node of a spring element
- χ_{LT} = Buckling factor (reduction factor for the beam resistance due to lateral-torsional buckling)
- $\kappa_{LT,num}$ = Numerically determined buckling factor
- $\kappa_{LT,vm}$ = Buckling factor according to the proposed verification method
- λ_{LT} = Non-dimensional (relative) slenderness for lateral-torsional buckling
- μ = Mean value of the ratio between $\kappa_{LT,vm}$ and $\kappa_{LT,num}$
- σ = Standard deviation of the ratio between $\kappa_{LT,vm}$ and $\kappa_{LT,num}$
- σ_{ini} = Initial (residual) stress
- A = Cross-sectional area
- A₁-A₄ = Constants in the equation for the critical elastic buckling load of type 2/3 connections
- B₁-B₇ = Constants in the equation for the critical elastic buckling load of type 4 connections
- D₁-D₉ = Constants in the equation for the critical elastic buckling load of type 5 connections
- E = Young's modulus (Modulus of elasticity)
- G = Shear modulus
- F = Concentrated load
- I_t = Torsional constant
- I_{t,tot} = Torsional constant of a model consisting of shells and extra elements (beams and springs)

$I_{t,shell}$	=	Torsional constant of a model consisting of shells
$I_{t,spring}$	=	Converted 'torsional constant' of a spring element
I_{wa}	=	Warping constant
I_y	=	Second moment of inertia about the strong axis
I_z	=	Second moment of inertia about the weak axis
L	=	Beam span
M	=	Bending moment
M_{cr}	=	Critical elastic buckling load
M_{pl}	=	Plastic capacity
M_{Rd}	=	Buckling resistance
T	=	Torsional moment
T_{pl}	=	Plastic capacity for torsion
c	=	Cope length
d_c	=	Cope depth
e_b	=	Unsupported web height above the endplate (distance between bottom flange and lower side of the endplate)
e_u	=	Unsupported web height under the endplate (distance between upper flange and upper side of the endplate)
f_y	=	Yield stress
h	=	Section height
h_c	=	Height of the section in the coped region (=h-d _c)
h_e	=	Height of the endplate
k_{spring}	=	Rotational spring stiffness
l	=	Element length
u_y	=	Displacement in direction of the weak axis

Annex: Test program

For a further validation of the numerical models, tests were carried out. This Annex gives an overview of these tests. The test set-up developed in this research project is shown in figure 35.

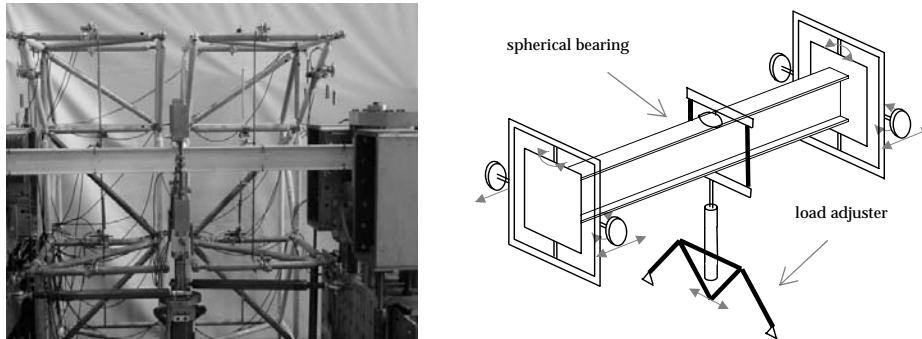


Figure 35: Test set-up

Cardan supports were developed to model simple supports, i.e. rotations about the weak and strong axes and translation in longitudinal direction are free and rotation about the longitudinal axis and translations in vertical and lateral direction are restrained at the supports, see figure 36. As soon as load is applied on the specimen, the specimen is stabilised in longitudinal direction. The static system is thus according to the left picture in figure 37. This corresponds to the right picture in figure 37.

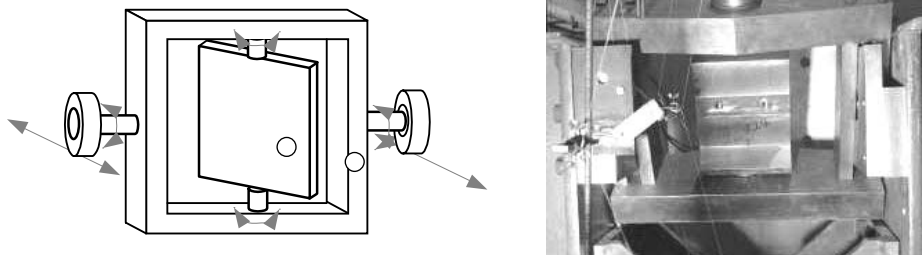


Figure 36: Cardan supports

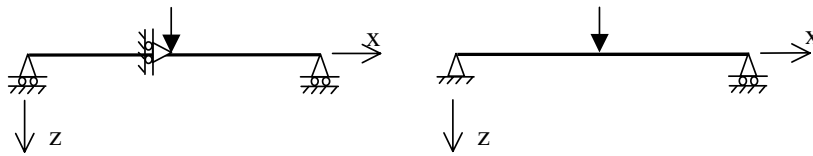


Figure 37: Static system (left: static system in the set-up, right: comparable static system)

A load adjuster and a spherical bearing were used to introduce the load. The spherical bearing consisted of a bowl and a sphere with grease in between. The radius of the sphere determines the load application point, see figure 38. For the tests, two spheres were developed, one for load application in the centre of the upper flange and one for load application in the centroid of the section. Figure 39 shows the functioning of the spherical bearing.

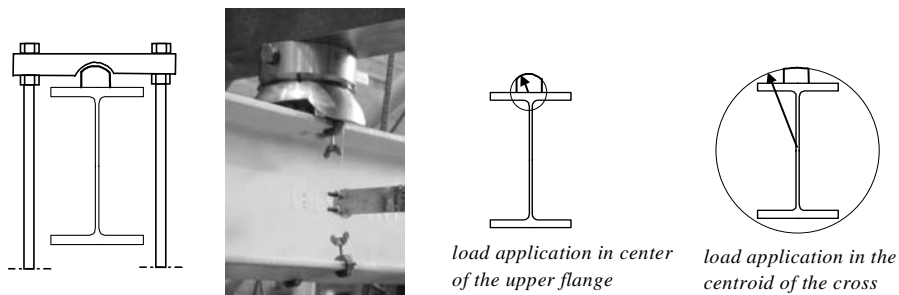


Figure 38: Spherical bearing

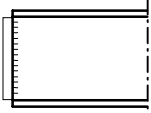
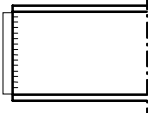
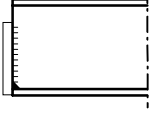
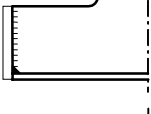
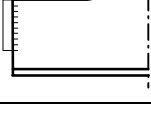


Figure 39: Functioning of the spherical bearing (left before testing, right during testing)

Ten IPE 120 beams with a span of 2,0 m and with type 1 to type 5 connections were tested. For these stocky beams with a relatively slender web, influence of the cope on the resistance of the beams is to be expected. During the test, lateral and vertical displacements of five cross-sections were measured, together with the load. The measured resistances of the tested beams are given in table 4.

Three tests failed because dents in the bowl of the spherical bearing prevented the rotation of the beam at the load introduction point. These tests are not included in table 4.

Table 4: Resistances for the tested beams

beam number	connection	load application	F_b [kN]
A1 (type 1 connection)		Upper flange	34.3
A2 (type 1 connection)		Upper flange	35.7
A3 (type 2 connection)		Upper flange	34.1
A4 (type 3 connection)		Upper flange	36.2
B1 (type 4 connection)		Upper flange	31.2
B2 (type 4 connection)		Centroid	28.4
B4 (type 5 connection)		Upper flange	25.1

The rotation of the cross-section at five locations of tests A3 (type 2 connection) and B1 (type 4 connection) are shown in figure 39. Large rotations occur in the coped regions. Extreme rotations in the coped regions were found for type five connections (see figure 40).

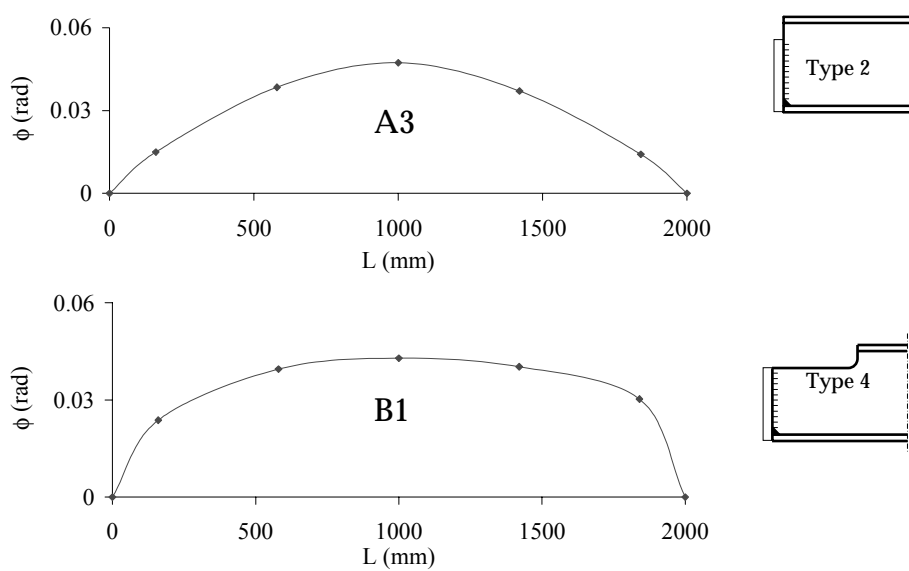


Figure 40: Rotation of five measured cross-sections of tests A3 (type 2) and B1 (type 4)

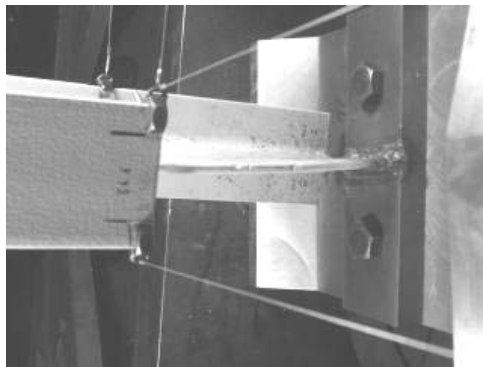


Figure 41: Rotation in the coped region of test B5 (type 5 connection) – top view

For a proper comparison between the numerical models and the tests, all relevant parameters of the tested beams should be known. The following parameters were considered.

- Span, cope dimensions and the dimensions of the cross-section are important parameters for both the critical elastic buckling load and the ultimate resistance. These properties were measured for each beam, before testing;

- In a numerical sensitivity analysis, it was determined that the size of the initial geometric imperfection (non-straightness of the beam) has a significant influence on the beam resistance. The initial imperfections were measured for each beam, before testing.
- The yield stress, ultimate tensile strength and Young's modulus were determined for the flanges and the web of each beam, after the beams were tested.
- In a numerical sensitivity analysis, it was determined that the magnitude of the residual stress has no significant influence on the beam resistance for the tested beams (a variation in the residual stresses of 10% resulted in a variation in resistance of 0,05% to 0,35%). Therefore, the residual stresses were not measured. The pattern according to figure 13 was applied.

Numerical models were made with these measured geometrical and physical properties. The initial geometric imperfection of beam A1 was not measured correctly. Therefore, it was not possible to simulate this beam.

The numerically determined resistances were 12% up to 25% lower than the tested resistances. In order to give an explanation for this significant difference, the friction between the bowl and the sphere was measured. For this purpose, a bowl was placed in between two identical spheres. The spheres were pressed with a load approximately equal to the maximum load in the experiments. The resistance against rotation of the bowl was then measured, see figure 41. The measured coefficient of friction was only 0,4 to 0,7 %, depending on the load and the side of rotation of the bowl. The friction in the cardan supports was so low, that it was not possible to measure it.

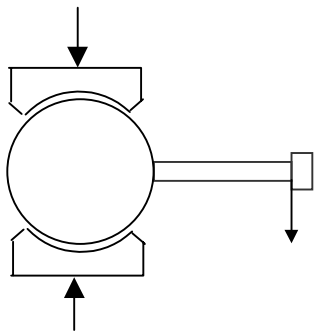


Figure 42: Set-up to determine friction in the spherical bearing

In order to determine the relation between friction in the load application and resistance, a sensitivity analysis was carried out numerically. For this purpose, a rotation spring with high elastic stiffness and a variable plastic limit was added in longitudinal direction at the point of load application to the numerical model of beam A4. Results are shown in figure 42.

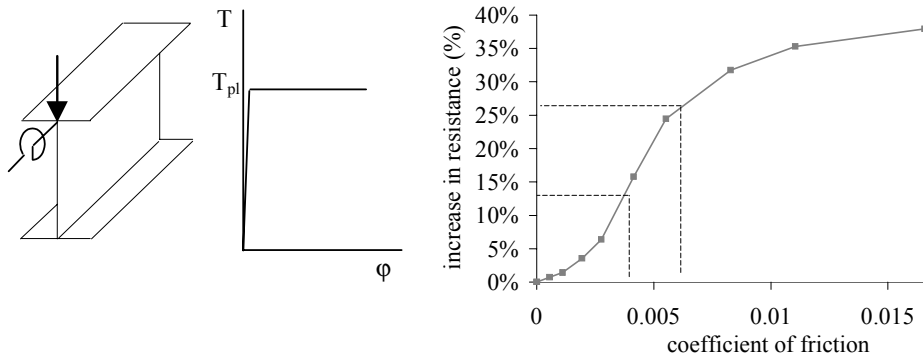


Figure 43: Influence of friction in load application on the beam resistance

Figure 43 shows that a very low friction in the load application causes an important increase in resistance. The difference between the numerically determined resistances and the tested resistances for the different beams was 12% to 25%. The coefficient of friction in the load application that causes this increase is 0,35% to 0,6% according to the figure. This corresponds reasonably with the measured coefficient of friction.

Although differences between numerically determined and tested resistances can be explained, a satisfactory validation with good agreement between tests and numerical models was not obtained.

In an additional research, the load application should be changed such, that the coefficient of friction is lower and that the load application also functions at high loads.

Conclusions from the laboratory tests are:

- Small differences in geometry are as important as the presence of partial endplates for the resistance, see Maljaars, 2001 (13);
- A relatively small friction in the load application improves the resistance to buckling significantly, causing a large increase in resistance. Such restraint is normally always present in practice.